Domain decomposition methods to model heat exchanges between a well and a rock mass

Roland Masson, Laurent Jeannin, Floriane Louvet, Aden Vuddamalay

Domain decomposition methods to model heat exchanges between a well and a rock mass

R. Masson*, L. Jeannin†F. Louvet ‡A. Vuddamalay §

February 19, 2020

Abstract

This paper focuses on the modelling of heat transfer between fluid flowing in a well and the surrounding rock mass and proposes an efficient domain decomposition approach to solve this problem. The importance of such a method is illustrated by the study of the modelling of underground gas storage in salt caverns.

1 Introduction

Gas underground storage in salt caverns is a mature technique, which ensures flexibility on the gas network and supplies security during the winter season. These caverns built by leaching behave as pressure vessels and may deliver high flow rates on demand. Natural gas is injected during summer and withdrawn during winter. Evolution of the gas market in the last few years, however, has changed the way the caverns were operated. They are now used more often with shorter cycles lasting a month, a week or less. In this context, it becomes very important to know and predict the thermodynamic state of gas at the wellhead and in the cavern. Modelling is used, on one hand, to predict the storage performance and improve its exploitation (to determine gas volume, hydrate risk, etc...) and on the other hand, to design surface facilities [18, 3, 17] during preliminary development studies. This last point also concerns storage of other gas such as H_2, that may be produced by electrolysis [21]. During operations, models are history-matched with available thermodynamic data (at the wellhead and in the cavern when available).

In this paper, we focus on the thermal modelling aspects of salt caverns operations and mainly on the numerical modelling of heat exchanges between the well and the rock mass nearby. Heterogenoeus domain decomposition methods (see e.g. [22], [10]) are investigated to couple at the well boundary the thermal evolution of a 1D well model with

*Université Côte d'Azur, CNRS, Inria team Coffee, LJAD, 06108 Nice, Cedex 02, France, roland.masson@univ-cotedazur.fr

†STORENGY, 12 rue Raoul Nordling - Djinn - CS 70001 92274 Bois Colombes Cedex, France, laurent.jeannin@storengy.com

‡STORENGY, 12 rue Raoul Nordling - Djinn - CS 70001 92274 Bois Colombes Cedex, France, floriane.louvet@storengy.com

§STORENGY, 12 rue Raoul Nordling - Djinn - CS 70001 92274 Bois Colombes Cedex, France, aden.vuddamalay@storengy.com

the surrouding 3D rock domain. These algorithms solve successively the well and rock mass subproblems until convergence to the fully coupled solution, the term heterogeneous refering to the fact that both subproblems are here of different types. Compared with a monolithic fully coupled Newton type algorithm, domain decomposition approaches have the advantage to be modular and to allow the use of efficient off-the-shelf solvers in each subdomain.

The convergence rate of domain decomposition methods depends crucially on the boundary conditions applied at the interface between both subdomains. In this work, we investigate Robin-Robin optimized Schwarz domain decomposition methods based on Robin boundary conditions for both subproblems [20, 13, 12, 11]. It will be compared with the more usual Dirichlet Neumann domain decomposition algorithm based on a Dirichlet boundary condition on the rock mass subproblem combined with a Neumann boundary condition on the well subproblem. The choice of the Robin coefficients as well as of the relaxation parameter for the Dirichlet Neumann algorithm are investigated both theoritically and numerically in order to improve the convergence rate of the domain decomposition algorithms.

Heterogeneous domain decomposition methods have previously been used to couple different physical models at the interface between subdomains. For example, let us refer to [7], [4], [8] for the coupling of a Darcy flow with a Stokes or Navier-Stokes free flow, to [2] for the coupling of non-isothermal liquid gas Darcy and free gas flows, and to [14] for the coupling of Helmholtz and Laplace Equations. Let us also refer to [1] and [23] for Robin-Robin domain decomposition methods developped for the nonlinear Richards equation modelling partially saturated flow in porous media.

The present work differs by the specific nature of the submodels and in particular by the different spatial dimensions of each subdomain. A specific and simple choice of the Robin coefficients will be shown to provide a very efficient convergence for this class of coupled models and for a large range of physical and numerical parameters.

The remainder of this paper is organized as follows. Section 2 presents the physical model describing fluid flow in the well and heat exchange with the surrounding rock mass. The next section investigates theoretically and numerically the convergence of the two domain decomposition methods for the well problem on a simplified linear case. For both algorithms, specific choices of the parameters are discussed in order to optimize the convergence of the algorithms. Numerical performance of both algorithms is evaluated. Finally, we consider the full problem of a cavern with a well and analyze the importance of heat exchange on synthetic cases and real data.

2 Modelling of thermodynamical gas behaviour of salt caverns

Underground gas storages in salt are connected to the surface through a well. During injection, gas is injected at the wellhead at a known flow rate and temperature and will flow downward through the well tubing into the cavern, which is generally at a few hundred meters to thousand meters depth. During withdrawal, gas is produced from the cavern at a given flow rate through the well.

Let ω_{well} denote the disk of $\mathbb{R}^2$ with radius r_w and centre the origin representing the section of the well. The well is assumed vertical; it is a cylindrical domain $\Omega_{\text{well}} = \omega_{\text{well}} \times (0, L)$. We denote by z the vertical coordinate oriented downward.

The surrounding rock domain is also assumed cylindrical to fix ideas although this assumption is not essential in what follows. It is denoted by $\Omega_{\text{rock}} = \omega_{\text{rock}} \times (0, L)$ with the rock section $\omega_{\text{rock}} = \omega \setminus \omega_{\text{well}}$ where $\omega \supset \omega_{\text{well}}$ is a simply connected domain of $\mathbb{R}^2$ (Fig. 1).

In the following, we denote by (r, θ, z) the cylindrical coordinates with respect to the well axis. The simulation time interval is denoted by $(0, t_f)$ with $t_f > 0$.

2.1 Well flow

We consider a one dimensional flow along the well which satisfies the following equations:
-gas equation of state

$$\frac{P}{\rho} = Z\ r\ T_{\text{ff}} \tag{1}$$

P denotes the gas pressure, T_{ff} the gas temperature, $Z(P, T_{\text{ff}})$ the compressibility factor, $\rho(P, T_{\text{ff}})$ the gas density in the well, and $r = \frac{R}{M_g}$ with R the ideal gas constant and M_g the gas molar mass.

-mass conservation
Mass flow rate is assumed constant along the well. In other words, we consider characteristic time greater than the propagation time of an acoustic wave along the well. With πr_w^2 the well section, Q the mass flow rate and u the gas velocity, it becomes:

$$u = \frac{Q}{\rho \pi r_w^2} \tag{2}$$

u and Q are assumed to be positive for injection and negative for withdrawal.

-momentum conservation
The velocity in the well is solution of the 1D momentum equation along the well, accounting for gravity and the pressure drop

$$\rho \frac{Du}{Dt} = -\frac{\partial P}{\partial z} + \rho g - sgn(u) \frac{\lambda}{2 r_w} \rho \frac{u^2}{2}$$

where λ is a friction coefficient estimated by the Colebrook [5, 6] and $\frac{D}{Dt} = \frac{\partial}{\partial t} + u \frac{\partial}{\partial z}$.

-energy conservation in the well.
Combining energy conservation and momentum conservation for the gas flow, we deduce the following equation:

$$\rho \frac{De}{Dt} = -P \frac{\partial u}{\partial z} + \frac{2}{r_w} \phi + \phi_v,$$

where e is the gas internal energy per mass unit, ϕ the heat flux at the wellbore accounting for convection and turbulence and ϕ_v the dissipation rate related to viscous effect.
Note that the average gas speed u is in the range 1-15 m.s^{-1}, thus gas flow is turbulent. This equation takes the following form:

$$\rho c_v^g \frac{DT_{\text{ff}}}{Dt} - T_{\text{ff}} \frac{\partial P}{\partial T_{\text{ff}}}|_\rho \frac{u}{\rho} \frac{\partial \rho}{\partial z} = \frac{2}{r_w} \phi + \phi_v,$$

with

$$\phi_v = -sgn(u)\frac{\lambda}{D}\rho\frac{u^3}{2},$$

and

$$\phi = \frac{1}{2\pi}\int_0^{2\pi} h(T_{wall}(\theta, z, t) - T_{\text{ff}}(z, t))d\theta,$$

c_v^g is gas heat capacity of the gas at constant volume per unit of mass. $T_{\text{wall}}(\theta, z, t)$ denotes the temperature on the wellbore, at the interface between the well and the rock mass.

h is the heat convective transfer coefficient given by:

$$h = \max(\frac{\lambda_g}{r_w}, \frac{\lambda_g}{2r_w}N_u) \tag{3}$$

where λ_g is the gas conductivity and N_u the Nusselt Number, which is estimated by the valid correlation for gas $N_u = 0.023Re^{0.8}Pr^{1/3}$ with Re the Reynolds number and Pr the Prandtl Number [15].

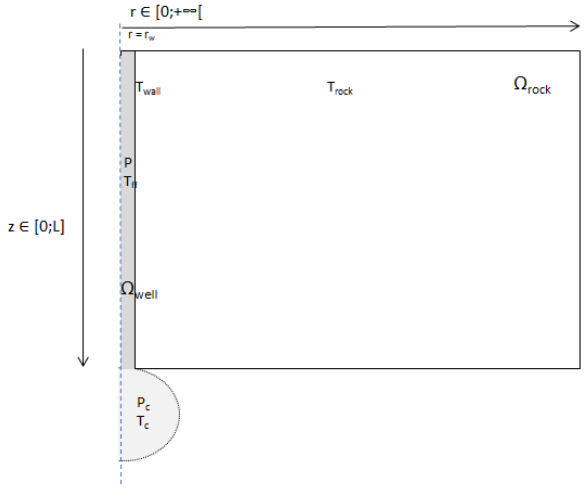

Figure 1: Axisymmetric diagram of the well-rock mass coupled problem - cavern (dotted line) will be considered in section 5

2.2 Rock mass surrounding well

Heat exchanges between the surrounding rock mass domain (denoted Ω_{rock}) may not be neglected. For example, gas may be heated up during withdrawal by the surrounding rock mass.

In the rock mass, the temperature field T_{rock} verifies the parabolic heat equation on $\Omega_{\text{rock}} \times (0, t_f)$:

$$\rho_r c_p^r \frac{\partial T_{\text{rock}}}{\partial t} + \text{div}\Big(-\lambda_{\text{rock}}\nabla T_{\text{rock}}\Big) = 0,$$

c_p^r is the specific heat capacity of the rock per unit mass, ρ_r the rock density and λ_{rock} the rock thermal conductivity,

At the interface between the well and rock domains, the following continuity of the temperatures and thermal fluxes is prescribed for all $(\theta, z, t) \in (0, 2\pi) \times (0, L) \times (0, t_f)$:

$$T_{\text{rock}}(r_w, \theta, z, t) = T_{\text{wall}}(\theta, z, t),$$
$$\lambda_{\text{rock}} \partial_r T_{\text{rock}}(r_w, \theta, z, t) = -h\Big(T_{\text{ff}}(z, t) - T_{\text{wall}}(\theta, z, t)\Big).$$

3 Domain decomposition methods applied to the well - rock mass domains

We analyze in this section two domain decomposition algorithms to solve the coupled well rock mass model. These methods solve iteratively the well and rock mass subproblems with transmission conditions chosen in order to obtain well-posed subproblems and to speed up the convergence to the coupled solution.

To study the convergence rate of the domain decomposition algorithms, we consider a simplified linear model for which the velocity in the well (and thus the density) is assumed to be constant (and not obtained from the solution of the 1D momentum equation as described in section 2). Then, the well energy equation is decoupled from the momentum conservation and reduces to a linear equation provided that the energy dissipation by friction is neglected. Note that c_v^g, h, c_p^r, ρ_r, and λ_{rock} are also assumed to be constant for this simplified model.

In order to apply a Fourier analysis in the z direction, the well axis is assumed to be the full line $\mathbb{R}$. For convenience, the rock domain is also assumed unbounded in the radial direction which is a valid approximation provided that the radius of the rock domain is large compared with r_w. It results that the cylindrical rock domain is defined in this section by $\Omega_{\text{rock}} = (r_w, +\infty) \times (0, 2\pi) \times \mathbb{R}$. Assuming an axisymmetric initial rock temperature, the solution of the coupled problem is axisymmetric. Then, the rock T_{rock}, well T_{ff} and wall T_{wall} temperatures are solutions of the following linear system of equations

$$\begin{aligned}
&\rho_r c_p^r \frac{\partial T_{\text{rock}}}{\partial t}(r, z, t) = \lambda_{\text{rock}} \Delta T_{\text{rock}}(r, z, t),\\
&\rho c_v^g \frac{\partial T_{\text{ff}}}{\partial t}(z, t) + \rho c_v^g u \frac{\partial T_{\text{ff}}}{\partial z}(z, t) = \frac{2}{r_w}\phi,\\
&T_{\text{rock}}(r_w, z, t) = T_{\text{wall}}(z, t),\\
&\lambda_{\text{rock}} \partial_r T_{\text{rock}}(r_w, z, t) = -h\Big(T_{\text{ff}}(z, t) - T_{\text{wall}}(z, t)\Big),
\end{aligned} \tag{4}$$

set on $(r, z, t) \in (r_w, +\infty) \times \mathbb{R} \times (0, t_f)$ and $(z, t) \in \mathbb{R} \times (0, t_f)$, using the fixed gas velocity u in the well, the coupling term

$$\frac{2}{r_w}\phi = H\Big(T_{\text{wall}}(z, t) - T_{\text{ff}}(z, t)\Big) \text{ with } H = \frac{2h}{r_w},$$

and given initial conditions for T_{rock} and T_{ff}.

The model is discretized in time using an Euler implicit integration scheme. Still denoting by $T_{\rm rock}$, $T_{\rm wall}$, $T_{\rm ff}$ the current time step temperatures and by $\widetilde{T}_{\rm rock}$, $\widetilde{T}_{\rm ff}$ the previous time step (or initial) rock and well temperatures, the semi-discrete system set on $(r,z) \in (r_w, +\infty) \times \mathbb{R}$ in the rock domain and on $z \in \mathbb{R}$ along the well reads:

$$\begin{aligned}
&(\eta - \lambda_{\rm rock}\Delta) T_{\rm rock}(r,z) = \eta \widetilde{T}_{\rm rock}(r,z),\\
&\eta^g T_{\rm ff} + \rho c_v^g u(T_{\rm ff})'(z) + \ H\Big(T_{\rm ff}(z) - T_{\rm wall}(z)\Big) = \eta^g \widetilde{T}_{\rm ff},\\
&T_{\rm rock}(r_w,z) = T_{\rm wall}(z),\\
&\lambda_{\rm rock}\partial_r T_{\rm rock}(r_w,z) = -h\Big(T_{\rm ff}(z) - T_{\rm wall}(z)\Big),
\end{aligned} \tag{5}$$

with the current time step Δt, and

$$\eta = \frac{\rho_r c_p^r}{\Delta t}, \quad \eta^g = \frac{\rho c_v^g}{\Delta t}.$$

3.1 Dirichlet Neumann algorithm

Let us consider the Dirichlet (on the rock side) Neumann (on the well side) domain decomposition algorithm, which updates $(T_{\rm wall}^{n-1}, T_{\rm rock}^{n-1})$ at iteration $n-1 \geq 0$ by $(T_{\rm wall}^{n}, T_{\rm rock}^{n})$ at iteration (n).
This algorithm solves the rock mass subproblem by imposing a Dirichlet temperature boundary condition at the wellbore given by the wall temperature of the well subproblem solution at the previous iteration (or by the wall temperature at the previous time step for $n = 0$). The thermal flux at the wellbore deduced from the rock subproblem solution is then imposed, as a Neumann boundary condition, to solve the well subproblem. In order to provide a more robust convergence, the Dirichlet Neumann algorithm classically needs to be relaxed (see e.g. [10]) using a relaxation parameter $\theta \in]0,1]$ as specified below. More specifically, the algorithm computes, at each iteration n, the solution $T_{\rm rock}^n$ of the the rock subproblem

$$\begin{cases}
(\eta - \lambda_{\rm rock}\Delta) T_{\rm rock}^n = \eta \widetilde{T}_{\rm rock} \text{ on } r_w, +\infty) \times \mathbb{R},\\
T_{\rm rock}^n(r_w,z) = T_{\rm wall}^{n-1}(z),\ z \in \mathbb{R},
\end{cases} \tag{6}$$

followed by the solution $\mathfrak{T}_{\rm ff}^n$ and $\mathfrak{T}_{\rm wall}^n$ of the well subproblem

$$\begin{cases}
\eta^g \mathfrak{T}_{\rm ff}^n(z) + \rho c_v^g u(\mathfrak{T}_{\rm ff}^n)'(z) + H\Big(\mathfrak{T}_{\rm ff}^n(z) - \mathfrak{T}_{\rm wall}^n(z)\Big) = \eta^g \widetilde{T}_{\rm ff},\ z \in \mathbb{R},\\
h\Big(\mathfrak{T}_{\rm ff}^n(z) - \mathfrak{T}_{\rm wall}^n(z)\Big) = -\lambda_{\rm rock}\partial_r T_{\rm rock}^n(r_w,z),\ z \in \mathbb{R},
\end{cases} \tag{7}$$

and the relaxation step

$$T_{\rm wall}^n(z) = \theta\ \mathfrak{T}_{\rm wall}^n(z) + (1-\theta) T_{\rm wall}^{n-1}(z),\ z \in \mathbb{R}. \tag{8}$$

3.1.1 Convergence rate

In order to study the convergence rate of this Dirichlet Neumann algorithm, we can assume, from the linearity of the equations, that $\widetilde{T}_{\text{rock}} = 0$ and $\widetilde{T}_{\text{ff}} = 0$. Then, starting from an arbitrary temperature error T^0_{wall}, the temperatures T^n_{wall}, T^n_{rock} represent the errors at iteration n. Following for example [10], the Fourier transform is applied in the z direction to the system (6)-(7)-(8) leading to the following transformed system

$$\begin{cases} \dfrac{\partial^2 \hat{T}^n_{\text{rock}}}{\partial r^2}(r,k) + \dfrac{1}{r}\dfrac{\partial \hat{T}^n_{\text{rock}}}{\partial r}(r,k) - (k^2 + \dfrac{\eta}{\lambda_{\text{rock}}})\hat{T}^n_{\text{rock}}(r,k) = 0, \\ \\ \hat{T}^n_{\text{rock}}(r_w,k) = \hat{T}^{n-1}_{\text{wall}}(k), \end{cases} \tag{9}$$

$$\begin{cases} (\eta^g + ik\rho c^g_v u)\hat{\mathfrak{T}}^n_{\text{ff}})(k) + H\Big(\hat{\mathfrak{T}}^n_{\text{ff}}(k) - \hat{\mathfrak{T}}^n_{\text{wall}}(k)\Big) = 0, \\ \\ h\Big(\hat{\mathfrak{T}}^n_{\text{ff}}(k) - \hat{\mathfrak{T}}^n_{\text{wall}}(k)\Big) = -\lambda_{\text{rock}}\partial_r \hat{T}^n_{\text{rock}}(r_w,k), \\ \\ \hat{T}^n_{\text{wall}}(k) = \theta\hat{\mathfrak{T}}^n_{\text{wall}}(k) + (1-\theta)\hat{T}^{n-1}_{\text{wall}}(k), \end{cases} \tag{10}$$

The solution $\hat{T}^n_{\text{rock}}$ of the first equation in (9) bounded for $r \to +\infty$ is expressed in terms of the second kind modified Bessel function K_m with $m = 0$ as follows:

$$\hat{T}^n_{\text{rock}}(r,k) = A^n(k)K_0(\mu(k)r), \tag{11}$$

with

$$\mu(k) = \sqrt{\frac{\eta}{\lambda_{\text{rock}}} + k^2}.$$

From the relation $K_0'(x) = -K_1(x)$, we note that

$$\lambda_{\text{rock}}\partial_r \hat{T}^n_{\text{rock}}(r_w,k) = -A^n(k)\lambda_{\text{rock}}\mu(k)K_1(\mu(k)r_w).$$

The Dirichlet Neumann algorithm then reduces to:

$$\begin{aligned} &K_0(\mu(k)r_w)A^n(k) = \hat{T}^{n-1}_{\text{wall}}(k), \\ &\Big(\eta^g + ik\rho c^g_v u\Big)\hat{\mathfrak{T}}^n{}_{\text{ff}}(k) + H(\hat{\mathfrak{T}}^n_{\text{ff}}(k) - \hat{\mathfrak{T}}^n_{\text{wall}}(k)) = 0, \\ &- h(\hat{\mathfrak{T}}^n_{\text{ff}}(k) - \hat{\mathfrak{T}}^n_{\text{wall}}(k)) = -\lambda_{\text{rock}}\mu(k)K_1(\mu(k)r_w)A^n(k), \\ &\hat{T}^n_{\text{wall}}(k) = \theta\hat{\mathfrak{T}}^n_{\text{wall}}(k) + (1-\theta)\hat{T}^{n-1}_{\text{wall}}(k), \end{aligned}$$

from which we deduce the following Fourier symbol of the iteration operator:

$$G_{DN}(k) = (1-\theta) - \theta\frac{\widehat{DtN}_{\text{rock}}(k)}{\widehat{DtN}_{\text{ff}}(k)}$$

such that

$$\hat{T}^n_{\text{wall}}(k) = G_{DN}(k)\hat{T}^{n-1}_{\text{wall}}(k),$$

with

$$\widehat{DtN}_{\text{rock}}(k) = \lambda_{\text{rock}}\mu(k)\frac{K_1(\mu(k)r_w)}{K_0(\mu(k)r_w)},$$
$$\widehat{DtN}_{\text{ff}}(k) = \frac{\eta^g + ikc_v^g u}{H + \eta^g + ikc_v^g u}\ h.$$

The function $\widehat{DtN}_{\text{rock}}(k)$ actually matches with the Fourier symbol of the rock subdomain Dirichlet Neumann operator defined by

$$g \to DtN_{\text{rock}}(g) = -\lambda_{\text{rock}}\partial_r T_{\text{rock}}(r_w, .), \tag{12}$$

where T_{rock} is the solution of the equation

$$\begin{aligned}&(\eta - \lambda_{\text{rock}}\Delta)T_{\text{rock}} = 0 \text{ on } (r_w, +\infty) \times \mathbb{R},\\ &T_{\text{rock}}(r_w, z) = g(z),\ z \in \mathbb{R}.\end{aligned} \tag{13}$$

This can be checked applying the Fourier transform in the z direction to (12)-(13) and using again the solution (11).

Likewise, $\widehat{DtN}_{\text{ff}}(k)$ matches with the Fourier symbol of the Dirichlet Neumann operator in the well subdomain defined by

$$g \to DtN_{\text{ff}}(g) = h\Big(T_{\text{wall}} - T_{\text{ff}}\Big), \tag{14}$$

with $(T_{\text{ff}}, T_{\text{wall}})$ solutions of the equation

$$\begin{aligned}&\eta^g T_{\text{ff}}(z) + c_v^g u(T_{\text{ff}})'(z) + H\Big(T_{\text{ff}}(z) - T_{\text{wall}}(z)\Big) = 0,\\ &T_{\text{wall}}(z) = g(z),\ z \in \mathbb{R}.\end{aligned} \tag{15}$$

This is also easily checked by applying the Fourier transform in the z direction to (14)-(15).

3.1.2 Choice of the relaxation parameter

The convergence of the Dirichlet Neumann algorithm will be obtained for a given frequency k if $|G_{DN}(k)| < 1$. The relaxation parameter $\theta \in]0, 1]$ should then be optimized to minimize the function

$$f_{DN}(\theta) = \max_{k \in (0, k_{max})} |G_{DN}(k)|,$$

with k_{max} depending on the spatial discretization along the well and typically given by $k_{max} = \frac{\pi}{\Delta z}$ where Δz is the spatial discretization step along the well assumed to be uniform. The optimal choice of θ seems difficult to compute analytically. A suboptimal but simple choice of the relaxation parameter θ can be obtained by imposing that $G_{DN}(0) = 0$, leading to

$$\theta = \frac{1}{1 + \dfrac{\widehat{DtN}_{\text{rock}}(0)}{\widehat{DtN}_{\text{ff}}(0)}} = \frac{1}{1 + (\dfrac{H + \eta^g}{h\eta^g})\dfrac{K_1(r_w\sqrt{\frac{\eta}{\lambda_{\text{rock}}}})}{K_0(r_w\sqrt{\frac{\eta}{\lambda_{\text{rock}}}})}\sqrt{\eta\lambda_{\text{rock}}}}. \tag{16}$$

3.2 Robin Robin optimized Schwarz algorithm

Let us consider the Robin Robin Schwarz algorithm [13, 12, 11] with Robin coefficients $\beta_{\text{rock}} \geq 0$ and $\beta_{\text{ff}} \geq 0$, $\beta_{\text{rock}}\beta_{\text{ff}} \neq 0$, which updates the temperatures $(T_{\text{ff}}^{n-1}, T_{\text{wall}}^{n-1}, T_{\text{rock}}^{n-1})$ at iteration $n-1 \geq 0$ by the temperatures $(T_{\text{ff}}^{n}, T_{\text{wall}}^{n}, T_{\text{rock}}^{n})$. They are defined by the solution T_{rock}^{n} of the following rock subproblem with Robin condition at the well boundary:

$$\begin{cases} (\eta - \lambda_{\text{rock}}\Delta)T_{\text{rock}}^{n} = \eta\widetilde{T}_{\text{rock}} \text{ on } (r_w, +\infty) \times \mathbb{R}, \\ \\ \beta_{\text{ff}}T_{\text{rock}}^{n}(r_w, z) - \lambda_{\text{rock}}\partial_r T_{\text{rock}}^{n}(r_w, z) = \beta_{\text{ff}}T_{\text{wall}}^{n-1}(z) + h\Big(T_{\text{ff}}^{n-1}(z) - T_{\text{wall}}^{n-1}(z)\Big),\ z \in \mathbb{R}, \end{cases} \tag{17}$$

followed by the solution $(T_{\text{ff}}^{n}, T_{\text{wall}}^{n})$ of the following well subproblem with Robin wall boundary condition:

$$\begin{cases} \eta^g T_{\text{ff}}^{n}(z) + \rho c_v^g u(T_{\text{ff}}^{n})'(z) + H\Big(T_{\text{ff}}^{n}(z) - T_{\text{wall}}^{n}(z)\Big) = \eta^g \widetilde{T}_{\text{ff}}(z),\ z \in \mathbb{R}, \\ \\ \beta_{\text{rock}}T_{\text{wall}}^{n}(z) - h\Big(T_{\text{ff}}^{n}(z) - T_{\text{wall}}^{n}(z)\Big) = \beta_{\text{rock}}T_{\text{rock}}^{n}(r_w, z) + \lambda_{\text{rock}}\partial_r T_{\text{rock}}^{n}(r_w, z),\ z \in \mathbb{R}. \end{cases} \tag{18}$$

3.2.1 Convergence rate

The convergence analysis proceeds as previously, setting that $\widetilde{T}_{\text{rock}} = 0$ and $\widetilde{T}_{\text{ff}} = 0$ and applying the Fourier transforms in the z direction to the system (17)-(18). Using the Bessel function solution (11) in the rock subdomain, we obtain that

$$\Big(\beta_{\text{ff}}K_0(\mu(k)r_w) + \lambda_{\text{rock}}\mu(k)K_1(\mu(k)r_w)\Big)A^n(k) = \beta_{\text{ff}}\hat{T}_{\text{wall}}^{n-1}(k) + h\Big(\hat{T}_{\text{ff}}^{n-1}(k) - \hat{T}_{\text{wall}}^{n-1}(k)\Big),$$

$$\Big(\eta^g + ik\rho c_v^g u\Big)\hat{T}_{\text{ff}}^{n}(k) + H\Big(\hat{T}_{\text{ff}}^{n}(k) - \hat{T}_{\text{wall}}^{n}(k)\Big) = 0,$$

$$\beta_{\text{rock}}\hat{T}_{\text{wall}}^{n}(k) - h\Big(\hat{T}_{\text{ff}}^{n}(k) - \hat{T}_{\text{wall}}^{n}(k)\Big) = \Big(\beta_{\text{rock}}K_0(\mu(k)r_w) - \lambda_{\text{rock}}\mu(k)K_1(\mu(k)r_w)\Big)A^n(k),$$

where $\hat{T}_{\text{rock}}^{n}$, $\hat{T}_{\text{ff}}^{n}$, $\hat{T}_{\text{wall}}^{n}$ represent respectively the rock, well and wall Fourier transforms of the temperature errors at iteration n. It results that the Fourier symbol $G_{RR}(k)$ of the Robin Robin algorithm iteration operator, defined by

$$A^n(k) = G_{RR}(k)A^{n-1}(k),$$

is given by

$$G_{RR}(k) = \frac{\beta_{\text{rock}} - \widehat{DtN}_{\text{rock}}(k)}{\beta_{\text{ff}} + \widehat{DtN}_{\text{rock}}(k)} \times \frac{\beta_{\text{ff}} - \widehat{DtN}_{\text{ff}}(k)}{\beta_{\text{rock}} + \widehat{DtN}_{\text{ff}}(k)}.$$

3.2.2 Choice of the Robin coefficients

The parameters β_{rock} and β_{ff} should be optimized to minimize the function

$$f_{RR}(\beta_{\text{rock}}, \beta_{\text{ff}}) = \max_{k \in (0, k_{max})} |G_{RR}(k)|. \tag{19}$$

The analytical solution of this min max problem seems difficult to compute analytically, and a numerical computation is not convenient to implement. In the spirit of [2], we propose below a suboptimal, but simple choice. Let us choose for β_{rock} the so called Taylor 0th order approximation of $\widehat{DtN}_{\text{rock}}$ which is exact for the lower frequency $k = 0$ ie

$$\beta_{\text{rock}} = \widehat{DtN}_{\text{rock}}(0) = \frac{K_1(r_w\sqrt{\frac{\eta}{\lambda_{\text{rock}}}})}{K_0(r_w\sqrt{\frac{\eta}{\lambda_{\text{rock}}}})}\sqrt{\eta\lambda_{\text{rock}}}.$$

Assuming that

$$\eta^g + |k|c_v^g u >> H,$$

the choice of the Robin coefficient

$$\beta_{\text{ff}} = h,$$

provides a good approximation of the Dirichlet Neumann operator $\widehat{DtN}_{\text{ff}}$ in the well domain. These choices of the Robin coefficients ensure a good compromise between the low and high frequencies (Fig. 2 and 3) since it results:
- from $\beta_{\text{rock}} = \widehat{DtN}_{\text{rock}}(0)$ that $G_{RR}(0) = 0$
- from $\beta_{\text{ff}} = h$ that $\lim_{|k|\to+\infty} |G_{RR}(k)| = 0$.

To fix ideas, let us remark that if $r_w >> \frac{1}{\sqrt{\frac{\eta}{\lambda_{\text{rock}}}}}$, in the limit of a planar interface rather than a cylindrical interface, the following simpler expression is obtained for the Robin coefficients:

$$\beta_{\text{rock}} = \sqrt{\eta\lambda_{\text{rock}}} \text{ and } \beta_{\text{ff}} = h.$$

As will be shown in the next section, for small radius r_w, like in our application, this "planar interface" approximation leads to a clearly slower convergence than the one obtained by taking into account the Bessel correction.

3.2.3 Alternative choice to $\beta_{\text{ff}} = h$

The choice $\beta_{\text{ff}} = h$ presents the disavantage that it is not robust in the limit of very small or vanishing velocity u combined with very large time steps. This issue is easy to solve using the following alternative choice of β_{ff} as the minimizer of $|\beta_{\text{ff}} - \widehat{DtN}_{\text{ff}}(k_{max})|$ which is defined by

$$\beta_{\text{ff}} = \beta_{\text{ff}}^{(1)} = \frac{(\frac{r_w}{2}\rho c_v^g u)^2\frac{k_{max}^2}{h} + \eta^g\frac{r^w}{2}(1+\eta^g\frac{r_w}{2})}{(\frac{r_w}{2}\rho c_v^g u)^2\frac{k_{max}^2}{h^2} + (1+\eta^g\frac{r_w}{2})^2.}$$

Compared with the choice $\beta_{\text{ff}} = h$, it has the advantage to ensure that the convergence rate vanishes for the trivial case $u = 0$.

3.2.4 Interpretation and generalization of $\beta_{\text{rock}} = \widehat{DtN}_{\text{rock}}(0)$

The choice $\beta_{\text{rock}} = \widehat{DtN}_{\text{rock}}(0)$ has the key asset to extend readily to the case of non axisymmetric and bounded rock domain geometry with general outer boundary conditions.

This extension can also account for heterogeneous rock thermal conductivity, and for the specific spatial discretization used in the rock domain. The idea is to come back to the definition of $\widehat{DtN}_{\rm rock}(0)$ in the physical space. From its definition (12)-(13), it amounts to compute using the rock domain discretization, the temperature $T_{\rm rock}$ solution of

$$\begin{array}{l}(\eta - \lambda_{\rm rock}\Delta)T_{\rm rock} = 0, \ \text{ on } \Omega_{\rm rock},\\ \quad T_{\rm rock}(r_w,\theta,z) = 1,\ (\theta,z) \in (0,2\pi)\times(0,L),\end{array} \tag{20}$$

using a Dirichlet condition of 1 at the well boundary and homogeneous boundary conditions at the remaining boundaries (of the same type than the rock model but homogeneous). Then, we set

$$\beta_{\rm rock}(\theta,z) = -\lambda_{\rm rock}\partial_r T_{\rm rock}(r_w,\theta,z). \tag{21}$$

This approximation hence requires the solution of the linear reaction diffusion problem (20) using the rock domain discretization at the cost of say 1 iteration of the algorithm. It has to be recomputed each time the time step is changing.

3.3 Numerical investigation of the convergence rates of the Dirichlet Neumann and Robin Robin algorithms

In this subsection, we consider the fixed gas pressure $P = 100$ bar and temperature $T = 30\ ^o$C along the well. The gas density $\rho = \rho(P,T)$ is given by the perfect gas equation of state setting $Z = 1$ and using the gas molar mass $M_g = 0.016$ kg.mol^{-1} in (1). We consider a fixed normal flow rate along the well

$$Q_n = Q\frac{\rho_n}{3600\rho},$$

in normal m^3 (nm^3) per hour with $\rho_n = \rho(P_{atm},T_{atm})$, $P_{atm} = 10^5$ Pa, $T_{atm} = 27\ ^o$C, from which one can deduce the gas velocity u from (2) with $r_w = 0.05$ m. The gas heat convective transfer coefficient h is defined by (3) with $\lambda_g = 0.0402$ W.m^{-1}.K^{-1}, the Nusselt correlation $N_u = 0.022\ Re^{0.8}\ Pr^{0.6}$, $Re = \frac{2r_wQ}{\mu_g}$, $Pr = \frac{c_v^g\mu_g}{\lambda_g}$ with $c_v^g = 1770$ J.K^{-1}.kg^{-1}, $\mu_g = 12.43\ 10^{-6}$ Pa.s. In the rock mass, we set $\lambda_{\rm rock} = 3$ W.m^{-1}.K^{-1}, $c_p^r = 800$ J.K^{-1}.kg^{-1}, $\rho_r = 2000$ kg.m^{-3}.

The following test cases investigate the convergence rates of the Robin Robin and Dirichlet Neumann algorithms depending on the normal flow rate Q_n in the range $[0, 150000]$ nm^3.h^{-1} and the time step Δt in the range [0.5 h, 1 year]. The maximum frequency $k_{max} = \frac{\pi}{\Delta z}$ is computed given a well lengh $L = 1500$ m and $N = 200$ uniform space steps of size $\Delta z = \frac{L}{N}$.

Figures 2 and 3 exhibit clearly that the Robin Robin algorithm is much more efficient than the Dirichlet Neumann algorithm and provides a very good contraction property. On the other hand, the Dirichlet Neumann algorithm provides a very poor contraction property and is not robust with respect to the physical parameters. This is an expected behavior of the Dirichlet Neumann algorithm for subproblems with highly contrasted geometries and physical properties as this is the case here.

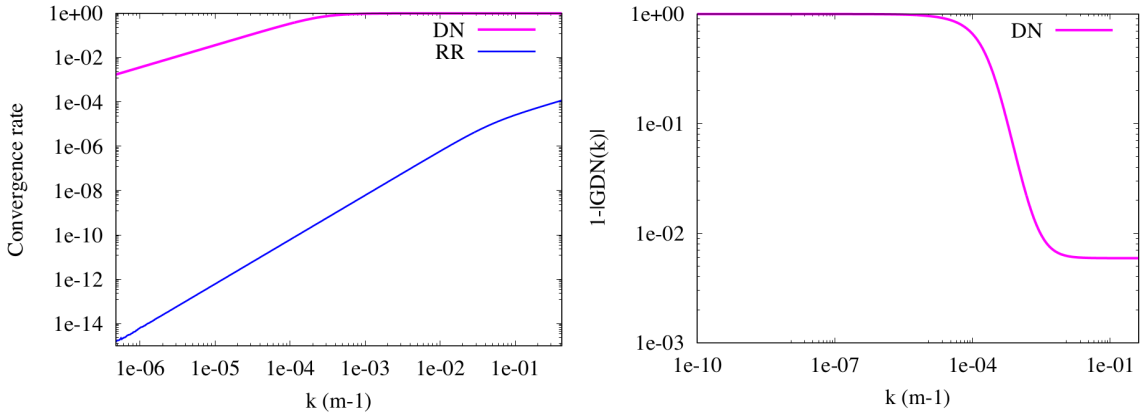

Figure 2: Both $|G_{RR}(k)|$ and $|G_{DN}(k)|$ (top) and $1 - |G_{DN}(k)|$ (bottom) as a function of $k \in [0, k_{max}]$ obtained with $Q_n = 30000$ nm^3.h^{-1}, $\Delta t = 6$ h and with $\beta_{\text{ff}} = h$, $\beta_{\text{rock}} = \widehat{DtN}_{\text{rock}}(0)$, θ given by (16). Note that $|G_{RR}(0)| = |G_{DN}(0)| = 0$.

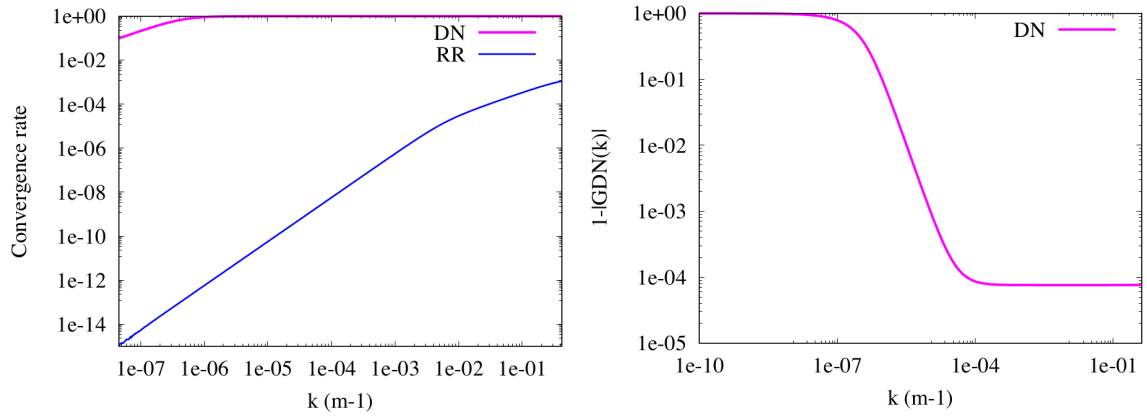

Figure 3: Both $|G_{RR}(k)|$ and $|G_{DN}(k)|$ (top) and $1 - |G_{DN}(k)|$ (bottom) as a function of $k \in [0, k_{max}]$ obtained with $Q_n = 150000$ nm^3.h^{-1}, $\Delta t = 30$ days and with $\beta_{\text{ff}} = h$, $\beta_{\text{rock}} = \widehat{DtN}_{\text{rock}}(0)$, θ given by (16). Note that $|G_{RR}(0)| = |G_{DN}(0)| = 0$.

Figures 4 and 5 compare our choices of the Robin coefficients with the ones obtained by a numerical approximation of the min-max problem

$$(\beta_{\text{rock}}, \beta_{\text{ff}}) = \text{argmax}_{(\beta_{\text{rock}} \geq 0, \beta_{\text{ff}} \geq 0)} f_{RR}(\beta_{\text{rock}}, \beta_{\text{ff}}).$$

This numerical approximate solution is obtained using a nonlinear optimisation algorithm starting from the initial guess given by ($\beta_{\text{rock}} = \widehat{DtN}_{\text{rock}}(0)$, $\beta_{\text{ff}} = h$) or by ($\beta_{\text{rock}} = \widehat{DtN}_{\text{rock}}(0)$, $\beta_{\text{ff}} = \beta_{\text{ff}}^{(1)}$) and retaining the best of the two solutions.

For the normal flow rates $Q_n = 30000$ nm^3.h^{-1} and $Q_n = 150000$ nm^3.h^{-1} , Figure 4 exhibits a typical behavior of the min-max solution characterized by an equi-oscillation of $|G_{RR}(k)|$ between $|G_{RR}(0)|$ and $|G_{RR}(k_{max})|$. This is clearly not the case for our choices since $\beta_{\text{rock}} = \widehat{DtN}_{\text{rock}}(0)$ ensures that $|G_{RR}(0)| = 0$. We note however that the values of $\max_{k \in (0, k_{max})} |G_{RR}(k)|$ are very close for the three choices of the Robin coefficients and for both test cases with $Q_n = 30000$ nm^3.h^{-1} and $Q_n = 150000$ nm^3.h^{-1}. As exhibited in

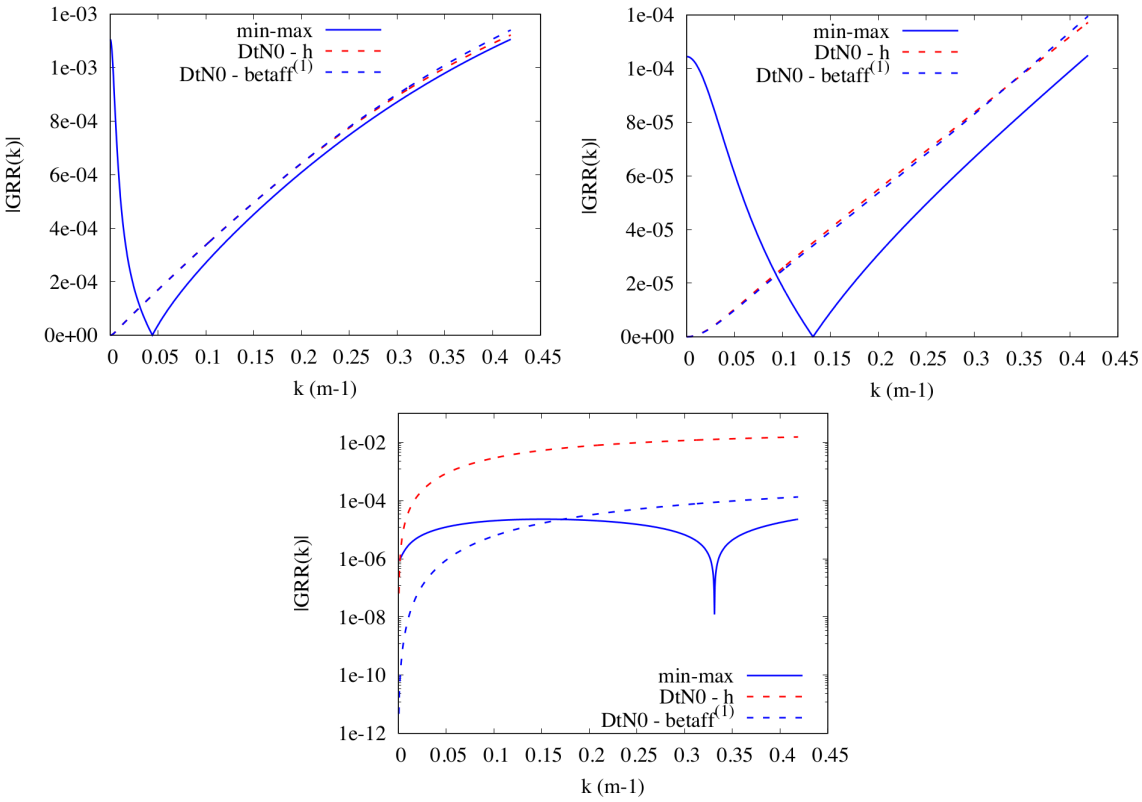

Figure 4: $|G_{RR}(k)|$ as a function of $k \in [0, k_{max}]$ obtained with the Robin coefficients given by a numerical approximation of the min-max problem, by the choice $\beta_{\text{rock}} = \widehat{DtN}_{\text{rock}}(0)$, $\beta_{\text{ff}} = h$ (denoted DtN0-h) and by the choice $\beta_{\text{rock}} = \widehat{DtN}_{\text{rock}}(0)$, $\beta_{\text{ff}} = \beta_{\text{ff}}^{(1)}$ (denoted DtN0-$\beta_{\text{ff}}^{(1)}$). The data set is defined by $Q_n = 150000$ nm^3.h^{-1} and $\Delta t = 30$ days (top), $Q_n = 30000$ nm^3.h^{-1} and $\Delta t = 6$ h (middle), and by $Q_n = 1$ nm^3.h^{-1} and $\Delta t = 360$ days (bottom).

Figures 4 and 5, the choice $\beta_{\text{ff}} = \beta_{\text{ff}}^{(1)}$ provides, as expected, for vanishing or very small normal flow rates combined with very large time steps, a much better convergence rate than the one obtained with the choice $\beta_{\text{ff}} = h$. In practice such large time steps are not used which motivates that the simpler choice $\beta_{\text{ff}} = h$ is prefered in the next sections.

Figure 5 shows that the simple choices $\beta_{\text{rock}} = \widehat{DtN}_{\text{rock}}(0)$, $\beta_{\text{ff}} = h$ and $\beta_{\text{rock}} = \widehat{DtN}_{\text{rock}}(0)$, $\beta_{\text{ff}} = \beta_{\text{ff}}^{(1)}$ for very small flow rates and very large time steps provide very competitive convergence rates compared with our numerical approximation of the min-max problem. This holds for the full range of normal flow rates and time steps used in practice.

4 Applications to the well problem

The well problem presented in section 2 has been discretized using a finite volume discretization. The velocity in the well is not imposed but obtained from the solution of the 1D momentum equation. Fluid flow problem may easily be reduced to two equations,

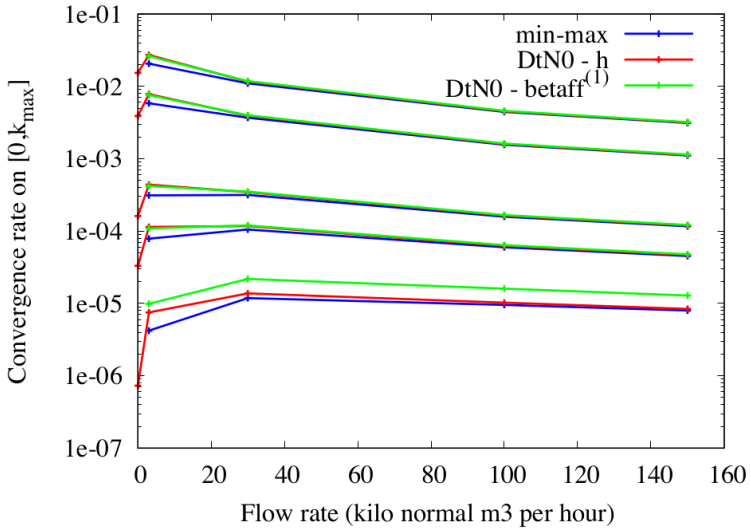

Figure 5: Convergence rate (defined as the maximum of $|G_{RR}(k)|$ in $k \in [0, k_{max}]$) as a function of the normal flow rate Q_n for the Robin coefficients obtained by a numerical approximation of the min-max problem (min-max), by the choice $\beta_{\text{rock}} = \widehat{DtN}_{\text{rock}}(0)$, $\beta_{\text{ff}} = h$ (denoted DtN0-h), and by the choice $\beta_{\text{rock}} = \widehat{DtN}_{\text{rock}}(0)$, $\beta_{\text{ff}} = \beta_{\text{ff}}^{(1)}$ (denoted DtN0-$\beta_{\text{ff}}^{(1)}$). The curves are plotted from bottom to top for the following values of the time step: $\Delta t = 0.5$ h, 6 h, 1 day, 1 month, 1 year. Note that the convergence rate for $Q_n = 0$ for the first and last cases is not plotted due to the log scale since it is vanishing.

derived from momentum and energy balance equation, depending on pressure and temperature in the well. The solution of the momentum equation and the energy balance equation are splitted in time. The Robin Robin and the Dirichlet Neumann algorithms for the time dependent problem have been implemented both for axisymmetric meshes and 3D radial meshes of the rock domain.

For the sake of clarity, we recall in the next section the finite volume discretization for axisymmetric meshes in the linear case studied in section 3 with a constant velocity $u \geq 0$ and constant density ρ, and we discuss a possible implementation of the domain decomposition algorithm.

4.1 Finite Volume Two Point Flux discretization for the axisymmetric model

We consider the following Cartesian mesh of the domain $(r_w, r_{max}) \times (0, L)$ defined by
$r_{i+1/2}, i = 0, \cdots, N_r$ such that $r_{1/2} = r_w$ and $r_{N_r+1/2} = r_{max}$, and by $z_{j+1/2}, j = 0, \cdots, N_z$ such that $z_{1/2} = 0$ and $z_{N_z+1/2} = L$.

Let us set

$$r_i = \frac{r_{i-1/2} + r_{i+1/2}}{2} \text{ for } i = 1, \cdots, N_r,$$

and

$$z_j = \frac{z_{j-1/2} + z_{j+1/2}}{2} \text{ for } j = 1, \cdots, N_z.$$

It is also convenient to set $r_0 = r_w$, $r_{N_r+1} = r_{max}$ and $z_0 = 0$, $z_{N_z+1} = L$.

The set of cells $K \in \mathcal{M}$ of the mesh is defined by

$$\mathcal{M} = \{K_{i,j} = (r_{i-1/2}, r_{i+1/2}) \times (z_{j-1/2}, z_{j+1/2}),\ i = 1, \cdots, N_r,\ j = 1, \cdots, N_z\},$$

and we define their volume by $|K_{i,j}| = (z_{j+1/2} - z_{j-1/2})\pi(r_{i+1/2}^2 - r_{i-1/2}^2)$. The set of faces $\sigma \in \mathcal{F}$ of the mesh is defined by

$$\begin{aligned}\mathcal{F} = &\left\{\sigma_{i+1/2,j} = \{r_{i+1/2}\} \times (z_{j-1/2}, z_{j+1/2}),\ i = 0, \cdots, N_r, j = 1, \cdots, N_z\right\} \\ &\cup \left\{\sigma_{i,j+1/2} = (r_{i-1/2}, r_{i+1/2}) \times \{z_{j+1/2}\},\ i = 1, \cdots, N_r, j = 0, \cdots, N_z\right\}.\end{aligned}$$

For $\sigma = \sigma_{i+1/2,j}$ we define the face surface and transmissibility

$$|\sigma| = 2\pi r_{i+1/2}(z_{j+1/2} - z_{j-1/2}),\ \tau_\sigma = \lambda_{\text{rock}}\frac{|\sigma|}{r_{i+1} - r_i},$$

and likewise for $\sigma = \sigma_{i,j+1/2}$ we define

$$|\sigma| = \pi(r_{i+1/2}^2 - r_{i-1/2}^2),\ \tau_\sigma = \lambda_{\text{rock}}\frac{|\sigma|}{z_{i+1} - z_i}.$$

We also denote by $\mathcal{F}_{int}$ the set of interior faces, and we set

$$\mathcal{F}_{ext} = \left\{\sigma_{N_r+1/2,j} = \{r_{N_r+1/2}\} \times (z_{j-1/2}, z_{j+1/2}),\ j = 1, \cdots, N_z\right\},$$

and

$$\mathcal{F}_{well} = \left\{\sigma_{1/2,j} = \{r_{1/2}\} \times (z_{j-1/2}, z_{j+1/2}),\ j = 1, \cdots, N_z\right\}.$$

Note that each face $\sigma = \sigma_{1/2,j} \in \mathcal{F}_{well}$ is associated to a unique well cell j for all $j = 1, \cdots, N_z$. The volume of the well cell j is denoted by

$$V_j = \pi r_w^2(z_{j+1/2} - z_{j-1/2}).$$

For all interior faces $\sigma \in \mathcal{F}_{int}$ we set $\sigma = KL$ meaning that the face is at the interface between cells K and L. Also, we denote by $\mathcal{F}_K \subset \mathcal{F}$ the subset of faces of the cell $K \in \mathcal{M}$. Note also that $|\sigma_{1/2,j}| = 2\pi r_w(z_{j+1/2} - z_{j-1/2})$ such that

$$\frac{|\sigma_{1/2,j}|}{V_j} = \frac{2}{r_w}.$$

Let be given the Dirichlet boundary conditions $T_{Dir,\sigma}$ for $\sigma \in \mathcal{F}_{ext}$ and assume for simplicity zero flux boundary conditions at the lower and bottom surfaces $z = 0$ and $z = L$. The Robin Robin algorithm solves iteratively the rock domain discrete system followed by the well discrete model, both using Robin condition at the well boundary. More specifically, the rock domain system discretizing (17) is defined by the conservation equation

$$\begin{aligned}&\eta|K|T_K^n + \sum_{\sigma = KL \in \mathcal{F}_K \cap \mathcal{F}_{int}} \tau_\sigma(T_K^n - T_L^n) + \sum_{\sigma \in \mathcal{F}_K \cap \mathcal{F}_{ext}} \tau_\sigma(T_K^n - T_{Dir,\sigma}) \\ &+ \sum_{\sigma \in \mathcal{F}_K \cap \mathcal{F}_{well}} \tau_\sigma(T_K^n - T_\sigma^n) = \eta|K|\widetilde{T}_K,\end{aligned}$$

in each cell $K \in \mathcal{M}$, combined with the Robin boundary condition

$$\beta_{\rm ff}|\sigma|T^n_\sigma + \tau_\sigma(T^n_\sigma - T^n_K) = \beta_{\rm ff}|\sigma|T^{n-1}_{{\rm wall},j} + h|\sigma|(T^{n-1}_{{\rm ff},j} - T^{n-1}_{{\rm wall},j}) := g^{n-1}_{{\rm ff},j},$$

for all $\sigma = \sigma_{1/2,j} \in \mathcal{F}_{well}$ using the right hand sides $g^{n-1}_{{\rm ff},j}$ computed from the well solution at the previous iteration. The well system discretizing (18) is defined by the conservation equation

$$V_j\eta^g_j T^n_{{\rm ff},j} + (\pi r_w^2)\rho c^g_v u(T^n_{{\rm ff},j} - T^n_{{\rm ff},j-1}) + |\sigma_{1/2,j}|h(T^n_{{\rm ff},j} - T^n_{{\rm wall},j}) = V_j\eta^g_j\widetilde{T}_{{\rm ff},j},$$

in each well cell $j = 1, \cdots, N_z$, combined with the Robin condition

$$\begin{aligned}\beta_{\rm rock}|\sigma_{1/2,j}|T^n_{{\rm wall},j} - h|\sigma_{1/2,j}|(T^n_{{\rm ff},j} - T^n_{{\rm wall},j}) &= \beta_{\rm rock}|\sigma_{1/2,j}|T^n_{\sigma_{1/2,j}} - \tau_{\sigma_{1/2,j}}(T^n_{\sigma_{1/2,j}} - T^n_K)\\ &:= g^n_{{\rm rock},\sigma_{1/2,j}},\end{aligned}$$

for all $j = 1, \cdots, N_z$ using the right hand sides $g^n_{{\rm rock},\sigma_{1/2,j}}$ computed from the previous rock domain solution.

The Robin coefficients are defined by

$$\beta_{\rm rock} = \frac{K_1(r_w\sqrt{\frac{\eta}{\lambda_{\rm rock}}})}{K_0(r_w\sqrt{\frac{\eta}{\lambda_{\rm rock}}})}\sqrt{\eta\lambda_{\rm rock}}, \tag{22}$$

and

$$\beta_{\rm ff} = h.$$

Given a specified tolerance ϵ, the algorithm is iterated until the stopping criteria $R^n \leq \epsilon$ is met with

$$R^n = \frac{\sum_{j=1}^{N_z}|T^n_{\sigma_{1/2,j}} - T^n_{{\rm wall},j}|}{\sum_{j=1}^{N_z}|T^n_{\sigma_{1/2,j}}|} + \frac{\sum_{j=1}^{N_z}|\Delta\Phi_j|}{\sum_{j=1}^{N_z}|\tau_{\sigma_{1/2,j}}(T^n_{\sigma_{1/2,j}} - T^n_K)|}, \tag{23}$$

using $\Delta\Phi_j = \tau_{\sigma_{1/2,j}}(T^{n+1}_{\sigma_{1/2,j}} - T^{n+1}_K) - h|\sigma_{1/2,j}|(T^{n+1}_{{\rm ff},j} - T^{n+1}_{{\rm wall},j})$.

From the implementation point of view, note that each rock temperature T^n_σ at the well faces $\sigma = \sigma_{1/2,j} \in \mathcal{F}_{well}$ can be locally eliminated using the Robin condition

$$\beta_{\rm ff}|\sigma|T^n_\sigma + \tau_\sigma(T^n_\sigma - T^n_K) = g^{n-1}_{{\rm ff},j},$$

leading to the flux

$$\tau_\sigma(T^n_K - T^n_\sigma) = \tau_\sigma\frac{\beta_{\rm ff}|\sigma|T^n_K - g^{n-1}_{{\rm ff},j}}{\tau_\sigma + \beta_{\rm ff}|\sigma|}.$$

It leads to solve a linear system with only the cell unknowns T^n_K for $K \in \mathcal{M}$. Likewise the wall temperatures $T^n_{{\rm wall},j}$ are locally eliminated using the Robin condition and right hand side $g^n_{{\rm rock},\sigma_{1/2,j}}$ leading to

$$T^n_{{\rm wall},j} = \frac{h|\sigma_{1/2,j}|T^n_{{\rm ff},j} + g^n_{{\rm rock},\sigma_{1/2,j}}}{\beta_{\rm rock}|\sigma_{1/2,j}| + h|\sigma_{1/2,j}|}.$$

Note that, in a more general case, the Robin coefficients could depend on the face σ due to the possible spatial dependence of η or $\lambda_{\rm rock}$ (see the next subsection for details). The Robin coefficient $\beta_{\rm rock}$ depends on time as soon as non uniform time steps are used and it has to be recomputed each time the time step is modified.

4.2 Numerical tests

We confirm by numerical experiments the results obtained in the Fourier space for the linear case (section 2).

- As a first example, we have assumed a constant flow rate per day during an injection sequence of a real gas during twelve days and have evaluated the robustness of each algorithm for different constant time-steps. The objective is to test the robustness of the algorithms on a range of flow rates and time steps, that will be used in practice for the modeling of cavern in operation.
The rock mass is assumed homogeneous with λ_{rock}= 5 W.K^{-1}.m^{-1}, c_p= 850 J.kg^{-1}.K^{-1}, ρ_{rock}= 2100 kg.m^{-3}. The initial temperature field in the rock mass is $T(z) = 20 + 0.029z$ in ^{o}C (geothermal gradient 29 ^{o}C/km). A constant heat flow is imposed at the bottom of the rock mass model, while surface temperature is assumed constant. A geothermal temperature profile is additionally imposed on the outer cylindrical surface (model is axisymmetric). The well is 1382 m long with a inner radius is 0.0871 m.
The temperature of the natural gas injected is assumed constant at the wellhead (20 ^{o}C) and the pressure at well bottom is assumed constant (200 bar).

The average number of iterations of domain decomposition for each algorithm has been reported (Tab. 1 to 5). The time to solution is proportional to the number of domain decomposition iterations. The numerical results show that Dirichlet Neumann algorithm, even when relaxed, is not robust (Tab. 4, 5). The most efficient algorithm is the Robin-Robin algorithm with coefficients β_{rock} and β_{ff} estimated on the radial geometry (Tab. 1). The simplified planar estimation of β_{rock} and β_{ff} converges but slowly (Tab. 3).

To quantify the quality of the solution as a function of the time step, we studied the deviation from the reference solution, chosen as the solution with a time step of 0.5h. The maximum well-bottom temperature and well-head pressure absolute difference are given in table 2.

- The next test cases consider the data set already defined in subsection 3.3, but here extended to a time dependent simulation taking into account variable density and velocity governed by the momentum and mass conservations coupled to the energy conservation along the well. The ideal gas is injected with a normal flow rate fixed to Q_n = 150000 nm^3.h^{-1} at a temperature $T = 30$ ^{o}C. The well bottom pressure is set to 100 bars. The temperature at the rock mass outer boundary as well as the initial rock temperature are both prescribed to $T(z) = 27 + 0.03z$ ^{o}C. During the simulation time of 10 years, the time step increases from an initial time step of 1800 s to a maximum time step of 6 months.

We consider first an axisymmetric simulation with an homogeneous rock thermal conductivity λ_{rock}= 3 W.K^{-1}.m^{-1} and a mesh of size 50×200 of the domain $(r_w, R_w) \times (0, L)$ exponentially refined at the well boundary with R_w = 10 m and L = 1500 m. Figure 6 compares the number of domain decomposition method (denoted DDM) iterations to reach the stopping criteria $R^n \leq \epsilon = 10^{-8}$ (see (23)) for the Robin coefficient $\beta_{\text{rock}} = \frac{K_1(r_w\sqrt{\frac{\eta}{\lambda_{\text{rock}}}})}{K_0(r_w\sqrt{\frac{\eta}{\lambda_{\text{rock}}}})}\sqrt{\eta\lambda_{\text{rock}}}$ and for β_{rock} obtained by the numerical solution (21)-(20).

Flow rate ($nm^3.h^{-1}$)	Iter. dt=.5(h)	Iter. dt=1(h)	Iter. dt=6(h)	Iter. dt=12(h)
0	1	1	1	1
500	4	4	4	4
1000	4	4	4	4
3000	5	5	4	4
6000	5	4	4	4
10000	5	4	4	4
12000	5	4	4	4
15000	5	4	4	3
20000	5	4	3	3
40000	5	4	3	3
80000	4	4	3	3
100000	4	4	3	3
120000	4	3	3	3

Table 1: Number of iterations for different flow rates for Robin Robin domain decomposition with coefficients given by Bessel function - $\epsilon = 10^{-8}$.

	Iter. dt=1(h)	Iter. dt=6(h)	Iter. dt=12(h)
max $\|T - T_{.5(h)}\|$ (^{o}C)	0.086	0.20	0.25
max $\|P - P_{.5(h)}\|$ (bar)	0.11	0.47	0.55

Table 2: Maximum well-bottom temperature and well-head pressure absolute difference with the 0.5(h) solution during the 12 days simulation.

This numerical computation of β_{rock} must be done at each time step in the case of a variable time stepping and has basically the cost of one DDM iteration. In both cases

Flow rate ($nm^3.h^{-1}$)	Iter. dt=.5(h)	Iter. dt=1(h)	Iter. dt=6(h)	Iter. dt=12(h)
0	1	1	1	1
500	5	5	15	23
1000	4	4	12	15
3000	9	9	16	17
6000	8	8	10	10
10000	7	7	8	7
12000	7	7	8	8
15000	7	7	7	8
20000	6	6	7	7
40000	5	5	5	7
80000	4	4	4	5
100000	4	4	4	4
120000	4	4	4	4

Table 3: Number of iterations for different flow rates for Robin Robin domain decomposition with coefficients given in the planar approximation - $\epsilon = 10^{-8}$.

Flow rate ($nm^3.h^{-1}$)	Iter. dt =.5(h)	Iter. dt =1(h)	Iter. dt =6(h)	Iter. dt =12(h)
0	n.c.	n.c.	n.c.	n.c.
500	n.c.	n.c.	n.c.	n.c.
1000	n.c.	n.c.	n.c.	n.c.
3000	n.c.	n.c.	n.c.	n.c.
6000	n.c.	n.c.	n.c.	n.c.
10000	n.c.	n.c.	18	18
12000	n.c.	n.c.	18	15
15000	n.c.	21	14	12
20000	20	18	12	12
40000	13	11	9	9
80000	10	8	7	6
100000	9	8	6	6
120000	8	7	6	6

Table 4: Number of iterations for different flow rates for Dirichlet Neumann domain decomposition - $\epsilon = 10^{-8}$.

Flow rate ($m^3.h^{-1}$)	Iter. dt =.5(h)	Iter. dt =1(h)	Iter. dt =6(h)
0	1	1	1
500	51	83	281
1000	52	85	279
3000	198	283	685
6000	200	281	685
10000	203	286	706
12000	204	287	708
15000	205	261	710
20000	205	287	714
40000	210	300	728
80000	219	308	737
100000	193	308	729
120000	191	308	718

Table 5: Number of iterations for different flow rates for relaxed Dirichlet Neumann domain decomposition - $\epsilon = 10^{-8}$.

we set $\beta_{\text{ff}} = h$. From Figure 6, we see that the numerical computation of β_{rock} presents a total gain of 154 DDM iterations over the full 98 time steps which amount to a net gain of say 56 DDM iterations compared with the analytical formula.

Figure 7 considers a 3D radial mesh of size $50 \times 50 \times 200$ of the rock mass domain $(r_w, R_w) \times (0, 2\pi) \times (0, L)$, $R_w = 10$ m, $L = 1500$ m, exponentially refined at the well boundary. The thermal conductivity is taken randomly in the interval $[2, 5]$ $\text{W.K}^{-1}.\text{m}^{-1}$ at each cell of the mesh. For such heterogeneous test case, the usual strategy is simply to use, at each face σ of the well boundary, the following value of the thermal conductivity

at the face σ:

$$\beta_{\mathrm{rock},\sigma} = \frac{K_1(r_w\sqrt{\frac{\eta}{\lambda_{\mathrm{rock},K}}})}{K_0(r_w\sqrt{\frac{\eta}{\lambda_{\mathrm{rock},K}}})}\sqrt{\eta\lambda_{\mathrm{rock},K}}, \tag{24}$$

with $\lambda_{\mathrm{rock},K}$ the value of λ_{rock} in the cell K with $\sigma \in \mathcal{F}_K$.

Alternatively, the numerical solution (21)-(20) takes into account the full heterogeneous thermal conductivity field and ensures that the convergence rate on the discrete linear coupled model vanishes for constant modes at the well boundary. From Figure 7, we observe a total gain of 149 DDM iterations for the numerical computation of $\beta_{\mathrm{rock},\sigma}$ compared with the analytical formula (24), providing a net gain of 51 DDM iterations for this variable time step simulation.

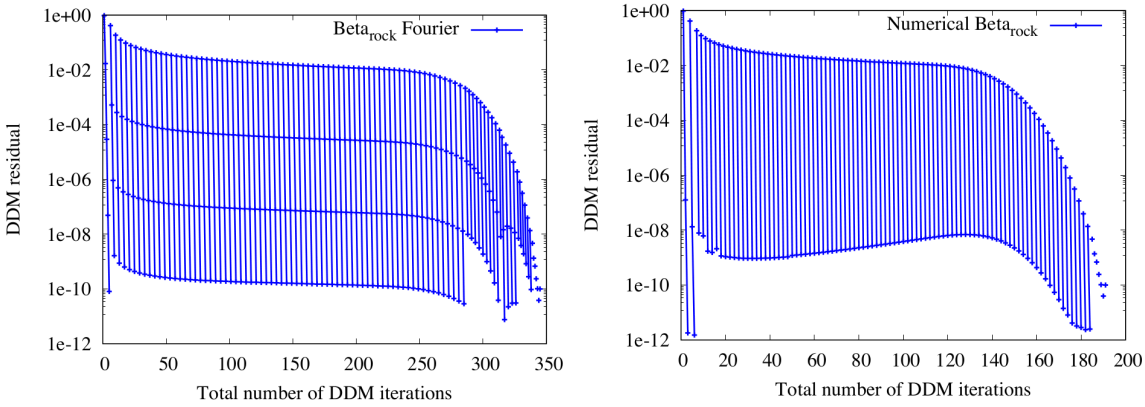

Figure 6: Convergence of the DDM residual (23) with one curve for each time step as a function of the cumulative number of DDM iterations for the axisymmetric test case with homogeneous thermal conductivity $\lambda_{\mathrm{rock}} = 3$ W.K^{-1}.m^{-1} on the mesh 50×200 with $Q_n = 150000$ nm^3.h^{-1}. (top): Fourier based definition of β_{rock}, (bottom): numerical computation of β_{rock}.

5 Salt cavern gas storage modelling

We apply our domain decomposition approach to the modelling of salt caverns gas storage.

5.1 Cavern model

Leaching operation makes it possible to build a cavern with a more or less cylindrical or spherical shape. Characteristic radius of the cavern is approximately 50m.
During storage operation, gas injection and withdrawal through the well induces compression or expansion of the gas into the cavern, and thus temperature changes of the gas. Inside the cavern, gas exchanges heat with the surrounding rock.

We choose in this study a simplified description of the cavern, where the gas pressure P_{c} and temperature T_{c} are assumed uniform in the cavern. The cavern will be considered

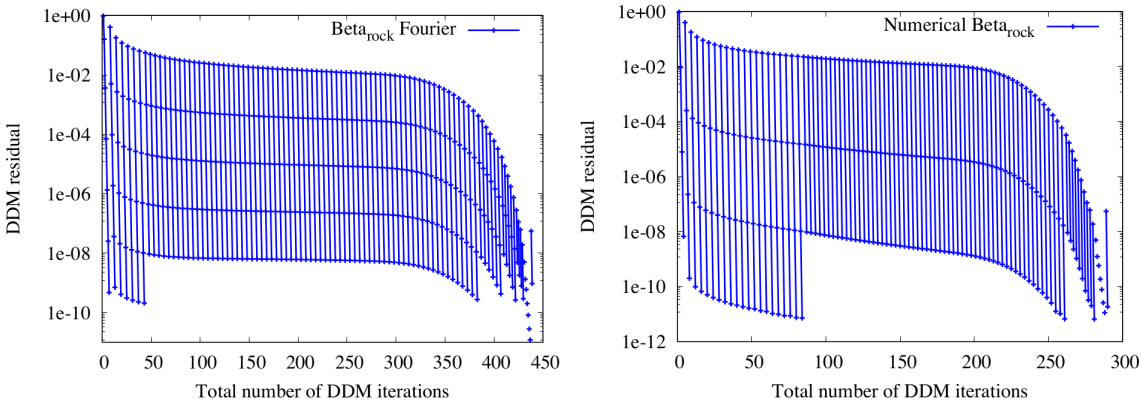

Figure 7: Convergence of the DDM residual (23) with one curve for each time step as a function of the cumulative number of DDM iterations for the 3D radial test case with random thermal conductivity $\lambda_{\text{rock}} \in [2, 5]$ W.K^{-1}.m^{-1} on the mesh $50 \times 50 \times 200$ with $Q_n = 150000$. (top): Fourier based definition of the face σ dependent Robin coefficient $\beta_{\text{rock},\sigma}$, (bottom): numerical computation of $\beta_{\text{rock},\sigma}$.

as a one dimensional spherical object of radius R_{cav}; moreover, the temperature field in the rock mass is assumed to have a spherical symmetry. V_{cav} denotes the cavern volume and S_{cav} its surface. Equations describing the thermodynamical evolution of the gas [9, 16] will be integrated on the cavern volume:
-mass conservation

$$\frac{\partial(\rho(P_c, T_c)V_{cav})}{\partial t} = Q$$

-energy balance equation in the cavern.
Using the second law of thermodynamics, it becomes:

$$(\rho c_v \frac{\partial T_c}{\partial t} - \frac{T_c}{\rho}\frac{\partial P}{\partial T}|_\rho \frac{\partial \rho}{\partial t})V_{cav} = \gamma S_{cav} h'(T_{wall,c} - T_c) + < Q >^+ c_p(T_{shoe} - T_c)$$

with

$$< Q >^+ = Q \text{ if } Q \geq 0$$
$$< Q >^+ = 0 \text{ if } Q \leq 0$$

γ is a shape surface factor, which reflects that the true surface of the cavern is not spherical. T_{shoe} is the gas temperature at the well bottom, c_p is gas specific heat capacity at constant pressure. h' is a heat transfer surface coefficient, which will depend on convection in the cavern and wall roughness and $T_{wall,c}$ represents the temperature at the cavern wall.
The first term of the r.h.s represents heat exchange with the rock mass surrounding the cavern, while the second term represents the heat input during injection.

One dimensional heat equation is solved in the rock mass. At the interface between cavern and rock mass, temperature fields and thermal fluxes are continuous.

5.2 Resolution

- cavern problem

We use a simplified discretization of the cavern problem, considering a spherical cavern embedded in a finite medium. The rock mass is indeed a spherical shell of large radius (larger than the length of diffusion during the cavern lifetime), typically of the order of 100m. It is discretized in spherical shells and a constant temperature is imposed on the outer surface. The cavern/rock mass problem is solved as a one dimensional coupled nonlinear problem. The rock mass initial temperature is assumed to be given by the geothermal temperature at the depth of the cavern centre.

-coupling well and cavern

Assuming pressure equilibrium between well bottom pressure and cavern pressure, the following relationship is obtained:

$$P_{shoe} = P_c + \rho(P_c, T_c) g R_{cav}$$

During injection, well and cavern problems are solved iteratively, as a fixed point problem, until convergence of P_{shoe} and T_{shoe} the pressure and temperature at the casing shoe. During withdrawal, cavern problem is solved first and $P_{shoe} = P_c + \rho(P_c, T_c) g R_{cav}$ and $T_{shoe} = T_c$ are imposed as boundary conditions at the well bottom.

5.3 Application to gas storage exploitation

- We first investigate the relevance of thermal exchange between well and rock mass. We consider a cavern with a volume of 275000 m^3 and an initial temperature of 62^{o}C and an inital pressure of 240 bars in the cavern. We assume a long withdrawal of 40000 $nm^3.h^{-1}$. We compare an adiabatic solution with no exchange between well and the rock mass, a solution with an infinite rock mass heat capacity (constant temperature in the rock mass) and the coupled solution obtained with the Robin Robin algorithm. The initial temperature field is the same as in the preceding paragraph. The rock thermal properties in the cavern model are the λ= 5.5 $W.K^{-1}.m^{-1}$, c_p= 920 $J.kg^{-1}.K^{-1}$, ρ_{rock}= 2100 $kg.m^{-3}$, while along the well λ= 5. $W.K^{-1}.m^{-1}$, c_p= 850 $J.kg^{-1}.K^{-1}$, ρ_{rock}= 2100 $kg.m^{-3}$.
  The convergence criterion of the decomposition domain algorithm is taken as ϵ=10^{-5} and time step is fixed to 6 hours. Number of iterations of domain decomposition algorithm for the coupled cases remains between 2 and 4.
  Figure 8 represents the temperature at the wellhead. The rock mass in the well vicinity heats up over time, as the gas is hotter than the surrounding rock mass near the wellhead. At the same time, the temperature inside the cavern is decreasing due to gas expansion in the cavern. Wellhead temperature evolution during the withdrawal may be compared with the adiabatic solution and the infinite rock heat capacity solution (Fig. 8). Wellhead temperature at the end of the withdrawal is close to the adiabatic one: due the relatively low value of thermal diffusion $d = \frac{\lambda}{\rho_{rock} c_p}$ in the rock mass , the rock mass temperature becomes close to the gas well temperature all along the well.

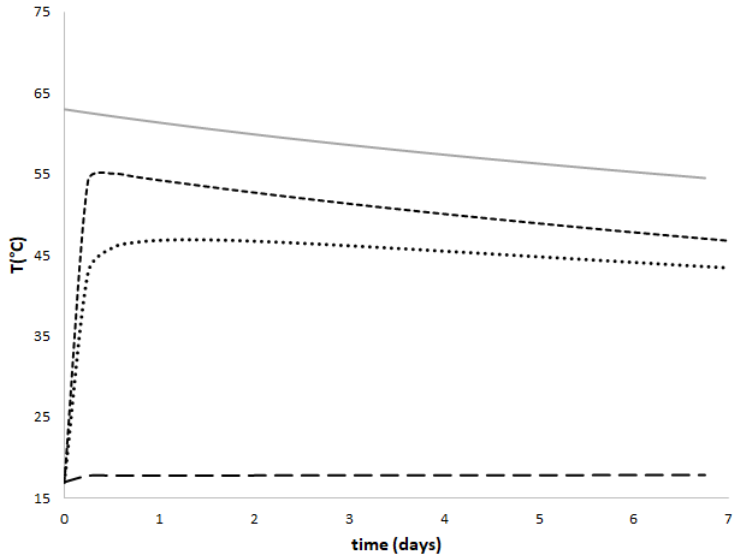

Figure 8: Wellhead temperatures for a long withdrawal at high flow rate - wellhead temperature for coupled case with finite rock mass heat capacity: dotted - wellhead temperature for adiabatic case: dashed line - wellhead temperature for infinite rock mass heat capacity: long dashed line - cavern temperature: grey line

- In the next example, a sequence made up of a withdrawal (during three days), a cavern rest (two days) and an injection (three days) is considered. Initial data and physical parameters are the same as in the preceding test. The temperature in the wellhead, accounting for heat exchanges with the rock mass, deviates significantly from the adiabatic solution and the solution with infinite heat capacity during the phases of withdrawal and rest. During injection, the injected gas temperature is imposed (at 20 ^{o}C). (Fig. 9). It can also be observed that the temperatures of the three solutions (coupled with finite rock mass heat capacity, adiabatic and infinite rock mass heat capacity) at the casing shoe (well bottom) differ significantly during the injection phase due to heat exchange in the well.
  Time step is fixed to 6 hours during injection and withdrawal and increased by a constant ratio of 1.2 at each time step during rest phase. ϵ is fixed at 10^{-5}. Number of iterations of domain decomposition algorithm for the coupled case remains between 2 and 4 as for the preceding test.

- Next figure illustrates the history-match of a true gas storage cavern (Fig. 10). Cavern modelling is used to predict cavern behavior during injection and withdrawal campaigns. A cavern model is built to reproduce the available data (wellhead pressure and temperature): the main calibration parameters of this history-matching approach are the shape factor of the cavern γ and the volume of the cavern [19]. ϵ is taken as 10^{-5} and the number of iterations of domain decomposition algorithm

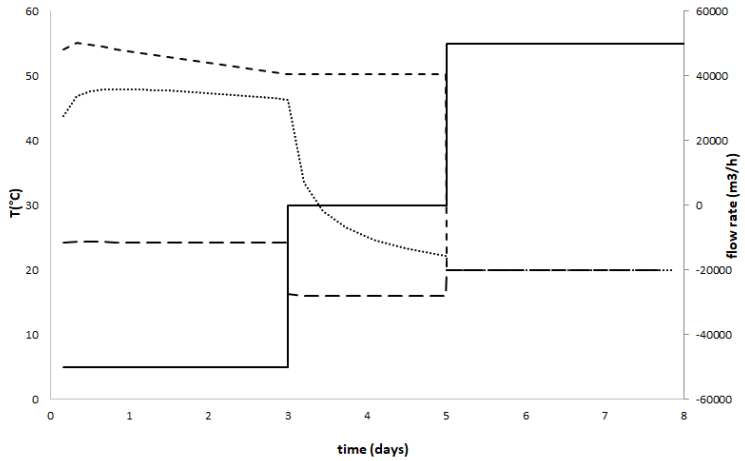

Figure 9: Wellhead temperatures during a sequence of injection and withdrawal - temperature for coupled case: dotted - temperature for adiabatic case: dashed line - temperature for infinite rock mass conductivity: long dashed line - flow rate: black line

for the coupled case remains limited to 2 to 4.
Wellhead pressure and temperature monitored have been plotted on Figure 10. Note that the estimated temperature is compared to measurements only when gas is withdrawn. Indeed during rest time, wellhead temperature is strongly dependent upon the weather; during injection, it is an input value.

6 Conclusion

This paper focuses on the modelling of heat transfer between fluid flowing in a well and the surrounding rock mass and proposes an efficient domain decomposition approach to solve this problem. The interest of such a method has been illustrated by the study of the modelling of underground gas storage in salt caverns.
The theoretical and numerical results show that the Dirichlet Neumann algorithm is not robust for this coupled model even with the introduction of a relaxation parameter. On the other hand, the Robin Robin algorithm provides a robust and efficient convergence for the range of physical parameters of interest including low flow rates and very small time steps. The Robin coefficient β_{rock} can be computed from the analytical formula obtained for an unbounded rock domain and for constant thermal conductivity and rock heat capacity. For heterogeneous thermal conductivity or rock heat capacity a better choice can be obtained by a numerical computation of β_{rock} at the cost of one iteration of the algorithm. The extension of this domain decomposition strategy to more complex well models, e.g. in geothermal systems, will be investigated in the near future.

Compared with a monolithic approach based on the solution of the fully coupled Jacobian system at each Newton iteration, the advantage of the nonlinear DDM is to allow the use of efficient off-the-shelf solvers on each subdomain. In our case we have

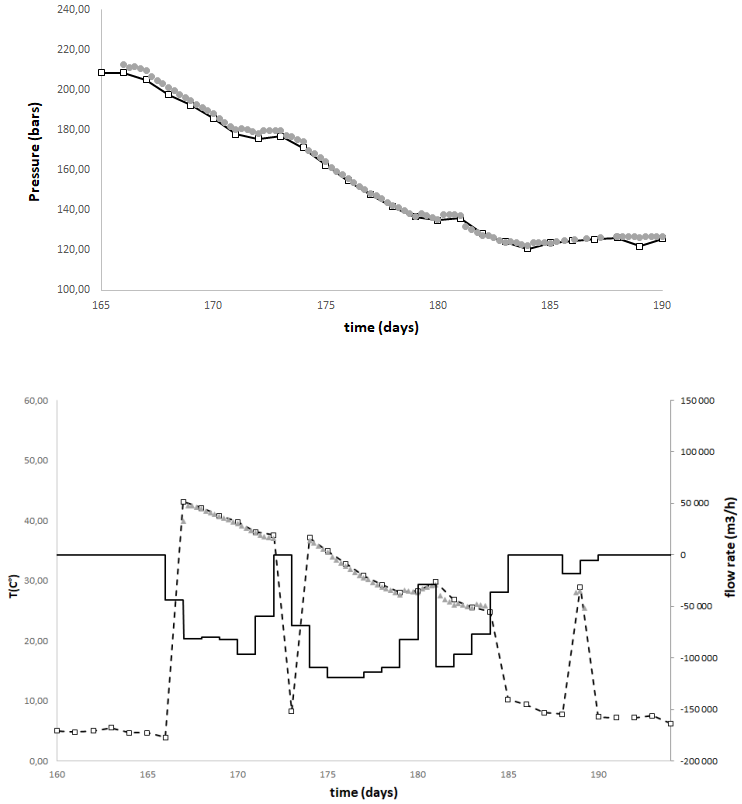

Figure 10: History-match of a cavern: Well-head pressure and temperature estimated by model (black marks) compared to availble data (grey marks) - flow rate (black line) is imposed in the model.

used a Conjugate Gradient algorithm preconditionned by an Algebraic MultiGrid (AMG) method for the rock linear subproblem and a local to each well cell Newton solver for the well nonlinear submodel, ordering the well cells in the flow direction. The monolithic approach would converge in a few Newton iterations making the total number of linear solves quite similar for both methods. On the other hand, the monolithic approach requires to design an efficient preconditioner for the fully coupled Jacobian system. This is not a trivial task considering the highly contrasted rock and well submodels both in terms of geometry and physics. A possible solution would be to apply the DDM algorithm to the fully coupled Jacobian system as a preconditioner combined with an approximate solve of the rock model based on a single AMG V-cycle. In other words, the domain decomposition method can also be exploited to make the monolithic approach more efficient.

References

[1] Berninger and Sanders, Substructuring of a Signorini-type problem and Robin's method for the Richards equation in heterogeneous soil, Computing and Visualization in Science, 13 (5), pp. 187-205, 2010.

[2] Birgle N., Masson R., Trenty L., A domain decomposition method to couple non-isothermal compositional gas liquid Darcy and free gas flows, Journal of Computational Physics, 368, pp. 210-235, 2018.

[3] Breheret C., Kelley K., Batson B., Optimizing Cavern Performance in Salt Gas Storage Thermodynamics, Modelling and Prediction, Pressure Maintenance, SMRI Spring 2013 Technical Conference, Lafayette, Apr. 2013.

[4] Cao Y., Gunzburger M., He X., and Wang X., Robin-Robin domain decomposition methods for the steady-state Stokes-Darcy system with the Beavers-Joseph interface condition, Numerische Mathematik, 117, pp. 601-629, 2011.

[5] Colebrook C.F. and White C.M., Experiments with Fluid Friction Factor in Roughened Pipes. Proceedings of the Royal Society of London. Series A: Mathematical and Physical Sciences, 161, 367-381, 1937.

[6] Colebrook C F., Turbulent flow in pipes with particular reference to the transition region between the smooth and rough pipe laws, J. Inst. Civil Engineers (London) 11 (4): 133-156, 1939.

[7] Discacciati M., Quarteroni, A., and Valli A., Robin-Robin Domain Decomposition Methods for the Stokes-Darcy Coupling, SIAM Journal on Numerical Analysis, 45, 3, pp. 1246-1268, 2007.

[8] Discacciati M., Giorda L.G., Optimized Schwarz methods for the Stokes-Darcy coupling. IMA J. Numer. Anal. 48, pp. 2091-2116, 2017

[9] Djizanne-Djakeun H., Stabilité mécanique d'une cavité saline soumise à des variations rapides de pression, PhD, Ecole polytechnique, 2014.

[10] DoleanV., Jolivet P. , Nataf F., An Introduction to Domain Decomposition Methods: Algorithms, Theory, and Parallel Implementation, SIAM publisher, 2015.

[11] Dubois O. and Gander M.J. , Optimized Schwarz methods for a diffusion problem with discontinuous coefficient, Numerical Algorithms, 69, 1, pp. 109-144, 2015.

[12] Dubois O., Optimized Schwarz methods with robin conditions for the advection-diffusion equation, in Domain Decomposition Methods in Science and Engineering XVI. Lecture Notes in Computational Science and Engineering, Springer, Berlin, 2006.

[13] Gander M.J. , Optimized Schwarz Methods, SIAM J. of Numerical Analysis, 44, 2, pp. 699-731, 2006.

[14] Gander M.J., Vanzan T. (2018) Heterogeneous Optimized Schwarz Methods for Coupling Helmholtz and Laplace Equations. In: Bjordstad P. et al. (eds) Domain Decomposition Methods in Science and Engineering XXIV. DD 2017. Lecture Notes in Computational Science and Engineering, vol 125. Springer, Cham

[15] Huetz J., Petit J.-P., Notions de transfert énergétique par convection, Techniques de l'ingénieur, 1990.

[16] Karimi-Jafari M., Sur le comportement transitoire des cavités salines profondes, PhD, Ecole polytechnique, 2007.

[17] Karimi-Jafari M., Thermodynamic simulation of gas caverns with GUSTS V.2, SMRI Fall 2016 technical conference, Salzburg, Sept. 2016.

[18] Klafki M., Wagler M., Thermodynamic Simulator KAVTEC for optimization of Gas Storage operation in salt saverns, SMRI Spring 2001 technical conference, Orlando, Apr. 2001.

[19] Krieter M., Dresen D., Influence of gas cavern's surface area on thermodynamic behaviour and operation, SMRI Fall 2011 technical conference, York, Oct. 2011.

[20] P.L. Lions, On the Schwarz alternating method. III: a variant for nonoverlapping subdomains, in 3rd International Symposium on Domain Decomposition Methods for Partial Differential Equations (Houston, TX, 1989), T. F. Chan, R. Glowinski, J. Périaux, and O. Widlund, eds., SIAM, Philadelphia, 1990.

[21] Nieland J.D., Salt cavern thermodynamics - comparison between hydrogen, natural gas and air storage, SMRI Fall 2008 technical conference, Galveston, Oct. 2008.

[22] A. Quateroni and A. Valli, Domain Decomposition Methods for Partial Differential Equations, Oxford University Press, 1999.

[23] D. Seus, K. Mitra, I.S. Pop, F.A. Radu, C. Rohde, A linear domain decomposition method for partially saturated flow in porous media, Computer Methods in Applied Mechanics and Engineering, 333, pp. 331-355, 2018.